# The time domain for brown dwarfs and directly imaged giant exoplanets: the power of variability monitoring

Astronomical Review

ISSN: 2167-2857 (Print) 2167-2865 (Online) Journal homepage: http://www.tandfonline.com/loi/tare20

# The time domain for brown dwarfs and directly imaged giant exoplanets: the power of variability monitoring

Beth Biller

**To cite this article:** Beth Biller (2017) The time domain for brown dwarfs and directly imaged giant exoplanets: the power of variability monitoring, Astronomical Review, 13:1, 1-27, DOI: 10.1080/21672857.2017.1303105

**To link to this article:** http://dx.doi.org/10.1080/21672857.2017.1303105



Published online: 10 Apr 2017.

ASTRONOMICAL REVIEW, 2017
VOL. 13, NO. 1, 1–27
https://doi.org/10.1080/21672857.2017.1303105

Taylor & Francis
Taylor & Francis Group



# The time domain for brown dwarfs and directly imaged giant exoplanets: the power of variability monitoring

Beth Biller

Institute for Astronomy, University of Edinburgh, Edinburgh, UK

**ABSTRACT**

Variability has now been robustly observed in a range of L and T type field brown dwarfs, primarily at near-IR and mid-IR wavelengths. The probable cause of this variability is surface inhomogeneities in the clouds of these objects (although other mechanisms may also contribute), causing a semi-periodic variability signal when combined with the rotational modulation from 3 to 20 h period expected for these objects. Variability at similar or even higher amplitudes has recently been observed in young brown dwarfs and planetary mass objects, which share similar $T_{\rm eff}$ as field brown dwarfs, but have considerably lower surface gravities. Variability studies of these objects relative to old field objects is then a direct probe of the effects of surface gravity on atmospheric structure.

**KEYWORDS**

Sections; lists; figures; tables; mathematics; fonts; references; appendices

## 1. Introduction

With near-IR multi-band imaging (and sometimes spectroscopy) in hand for ∼20 giant exoplanet companions, ∼30–40 free-floating young planetary mass objects, and >800 field brown dwarfs, we have learned a great deal about the atmospheres of self-luminous objects with masses of 3–80 $M_{\rm Jup}$, ages from 1 Myr to 10 Gyr, and surface gravities from $\log(g) =$ 3–5. These objects may have formed in diverse manners (some in disks around stars, others in isolation in the field), but fill out a grid of atmospheres with a range of masses, $T_{\rm eff}$, compositions, and surface gravities. To understand these objects as a class, we must study the full range of their atmospheres. Eventually we would hope to extend our studies down to cooler atmospheres around lower mass planets. In the coming decades, direct imaging of exoplanets will become a vital technique to detect and characterize Earth-like planets in the habitable zones around nearby M stars – current studies of giant exoplanets and brown dwarf atmospheres using this technique are thus precursors for similar studies for lower mass planets with future generations of telescopes.

Our knowledge of the atmospheres of 3–80 $M_{\rm Jup}$ atmospheres is drawn from photometric and spectroscopic studies. Workers in the field have compiled large compendiums of >1000 old field ultracool dwarf spectra (i.e. very low mass M stars as well as substellar objects, see e.g. Ref. [1]) and in-depth studies of younger, lower surface gravity spectra have

**CONTACT** Beth Biller bb@roe.ac.uk

recently been completed [2]. A handful of imaged planets now have low-resolution (R ∼30) spectroscopy in hand [3–10]. Based on these studies, old field brown dwarfs, young free-floating planetary mass objects, and exoplanet companions to stars are described using the same set of spectral types. Unlike stars which remain at the same effective temperature (henceforth $T_{\rm eff}$) for millions or billions of years due to nuclear core fusion, brown dwarfs and planetary mass objects alike cool monotonically with age, beginning life as hot M-type objects, cooling to the L spectral type (characterized by very red near-IR colors and silicate condensate clouds, [11]), the T spectral type (characterized by blue near-IR colors and strong methane absorption at 1.6 and 2.2 μm [11]), and eventually to the very cool Y spectral type [12,13] (see Figure 1). Thus, there is an age/mass/temperature degeneracy for these objects. Additionally, low surface gravity in younger and lower mass objects can significantly affect the spectra of these objects (and also the $T_{\rm eff}$) at which these objects transition between spectral types [14].

Most observations of brown dwarfs and planetary mass objects to date were acquired in a time-averaged and spatially unresolved manner – during a single observation that briefly probes one hemisphere. Variability monitoring is a powerful new method to study these atmospheres, which uses rotational modulation to probe different points on the surface of these objects. Detectable rotationally modulated variability in a specific class of object requires the presence of: (1) relatively short rotation periods (i.e. observable on the timescales of a night or two) and (2) surface inhomogeneities. Both of these conditions are fulfilled for brown dwarfs and young giant planets.

Condition 1 (short rotation periods) is clearly present in field brown dwarfs, which possess 3–20 h rotational periods. Zapatero Osorio et al. [15] obtained projected rotational velocities (*vsini*) for a sample of 19 M6.5-T8 very low mass stars and brown dwarfs using KECK NIRSPEC (see Figure 2). They found that the T dwarfs observed were generally faster rotators than the M stars in the sample. Assuming brown dwarfs are around ∼1 $R_{\rm Jup}$ in size (a reasonable assumption, given electron degeneracy in their cores, [16]), they find a maximum rotational period for their sample of L and T brown dwarfs of 12.5 h. It is important to note as a caveat that *vsini* may be somewhat overestimated for brown dwarfs (hence leading to a predicted rotation period shorter than the actual rotation period, as found for a few objects by [17]). This is because measuring *vsini* is spectral template dependent. For brown dwarf measurements, often the templates used are theoretical models which do not incorporate pressure broadening, thus requiring faster apparent rotation velocities to recover the measured line width. Nevertheless, while some rotation periods in an ensemble of objects such as that studied by [15] may be longer than predicted from the measured *vsini*, the conclusion that these objects are generally fast rotators (periods <20 h) still holds.

No similar survey of rotation periods has been completed for young L or T type brown dwarfs or planetary mass objects, but for the four measurements available to date of rotation periods for individual objects, three are fast rotators with periods of <11 h. Snellen et al. [18] measured a rotational velocity using VLT CRIRES for the 8–10 $M_{\rm Jup}$ planet $\beta$ Pic b [19]. This is the first rotational velocity measured for any extrasolar planet. In fact, $\beta$ Pic b rotates faster than any of the planets in the Solar system with $v_{\rm rotation} = 25 \pm 3\,{\rm km\,s^{-1}}$. Using spectral modeling from broadband photometry to infer a radius of $1.65 \pm 0.06\,R_{\rm Jup}$, this gives a rotational period of $\sim 8.1 \pm 1.0$ h. The same technique was used with the young substellar companion GQ Lupi B (with a higher estimated mass of ∼30–40 $M_{\rm Jup}$) yielding a considerably slower rotational period of ∼8 days [20]. Periods for two other planetary

mass objects have been measured directly from their observed periodic variability – the young planetary mass companion 2M1207b has a period of 11 h [21] and the free-floating young planetary mass object PSO J318.5-22 has a period of 5–10 h [22,23], see Figure 3. Overall, younger objects might be expected to have longer rotation periods relative to older objects due to conservation of angular momentum as these objects contract and spin up with age. However, at least preliminarily, some lower mass and younger objects appear to have relatively short periods.

There is significant evidence for surface inhomogeneities in these objects as well. In the case of objects with spectral types >L2, a likely source of surface inhomogeneities is patchiness in cloud cover or even multiple cloud components, especially at the L/T spectral type transition. Marley et al. [24] find that patchy cloud models best bridge the transition between the L and T spectral types, with entirely clear models best describing the later T spectral types and single component, entirely cloudy models best describing the earlier L spectral types (see Figure 4). Observationally, Skemer et al. [25,26] find that patchy cloud coverage may be required to model observations across a wide wavelength range. Temperature perturbations [27] and thermochemical instabilities [28,29] have also been proposed as variability mechanisms in L, T, and Y spectral type objects. For early L and late M objects, aurorae may be another driver of periodic variability [30]. Earlier spectral types (e.g. M type brown dwarfs in young star-forming regions such as Taurus) may also have variability dominated by mechanisms other than clouds: e.g. accretion from a circum-brown-dwarf or circum-planetary disk or magnetic phenomena such as starspots [31–34]. In contrast, L, T, and Y type brown dwarfs are too cool to have significant magnetically driven starspots and are more likely to have cloud-driven variability [35].

Spectroscopic variability monitoring in particular, e.g. searching for variability in specific spectral features, is a powerful test of model predictions. Overall, time resolved observations open up a new realm of potential characterization, enabling in some cases *spatial* resolution of surface features.

## 2. Current state of the art for brown dwarf variability monitoring

### *2.1. First steps*

Almost as soon as they were discovered, variability studies were attempted for L and T type brown dwarfs [35,40–56]. The first studies focused primarily on early L dwarfs in the red optical and suffered from the fact that these objects are predominantly faint at these wavelengths. These searches sometimes yielded inconsistent results – for instance, Gelino et al. [35] claim a period of 31 h for the L0.5 dwarf 2M0746+2000. However, Bailer-Jones [55] measure *vsini* $\sim$25–27 km s$^{-1}$ for this object, similar to what was later measured for the exoplanet $\beta$ Pic b (with a period of 7–9 h), thus suggesting a significantly shorter period.

In parallel, young brown dwarfs in star-forming regions such as Taurus were also searched for variability [31–34]. At ages <1 Myr, these objects are still quite hot and possess M spectral types. Thus, their variability is likely driven by mechanisms such as accretion from a circum-brown-dwarf or circum-planetary disk or magnetic phenomena such as starspots. Much of the activity found here is flaring and non-periodic, and likely has more in common with magnetically driven variability as seen on M stars than the sort of variability now commonly found in cooler L, T, and Y brown dwarfs.

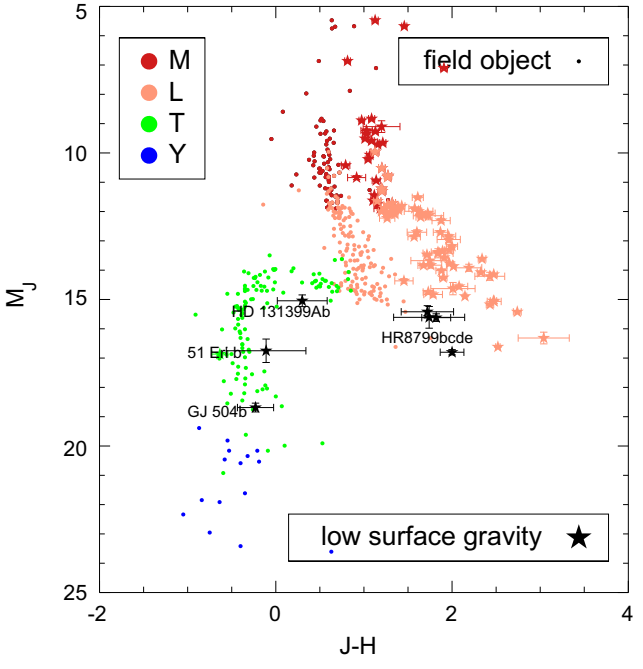


**Figure 1.** Color magnitude diagram using data from the compilations of [36–38], showing the locus of L and T field dwarfs, as well as low surface gravity objects with similar spectral types and directly imaged exoplanet companions data from [4,9,10,39].

Notes: The cooler T type brown dwarfs are notably bluer than the red Ls, due to significant methane absorption at 2.2 μm as well as the breaking up or sinking of silicate clouds below the photosphere. Low surface gravity objects are uniformly redder than objects with similar spectral types at field ages. Note the small population of extremely red exoplanets with 'T dwarf' luminosities, such as HR 8799bcde. These planets retain silicate clouds at considerably cooler temperatures than their brown dwarf counterparts, likely a result of their low surface gravities.

### *2.2. The detection of highly variable objects*

Concerns about the repeatability and significance of positive variability detections were allayed by the discovery of three high amplitude variables, specifically the T2.5 brown dwarf SIMP J013656.5+093347, the T1.5 brown dwarf 2MASS J21392676+0220226, and the T0.5 brown dwarf Luhman 16B, see Figure 5. While the amplitude of variability of these objects changes on very short timescales and may even vary from night to night, they display robust variability overall, with clear periodicity (suggesting variability is produced by rotational modulation of inhomogeneous but changing surface features). Interestingly, all three of these objects fall around the transition between L and T spectral type brown dwarfs – a transition over which the thick clouds emblematic of the L spectral type must somehow disperse by the mid to late T spectral type. The T2.5 brown dwarf SIMP J013656.5+093347 [57, hereafter SIMP 0136] is one of the brightest T dwarfs known and is the brightest such object in the northern hemisphere [58] found near-IR (J and $K_S$) variability in this object with a period of ∼2.4 h and a maximum amplitude of ∼50 mmag. This variability showed significant evolution from night to night and a larger overall amplitude in J than $K_S$. The ratio of the amplitudes in these bands can be used to put constraints on the physical mechanisms driving the observed variability – this will be discussed in greater detail in Section 2.5.

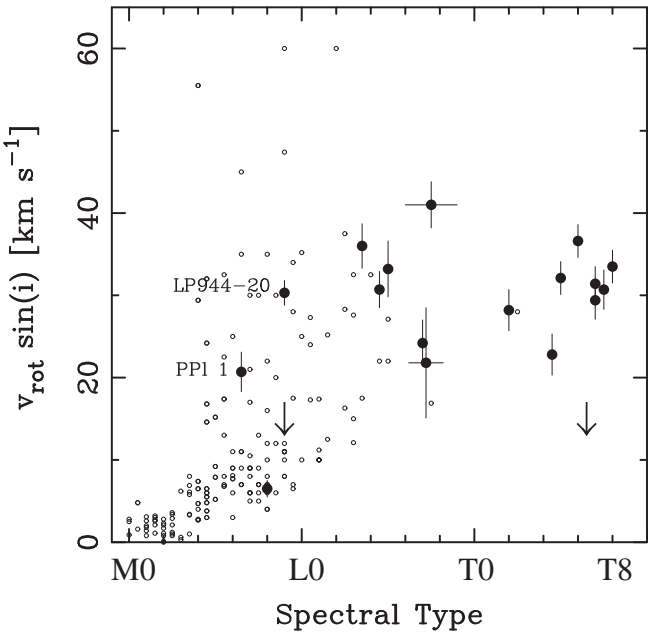


**Figure 2.** Figure from [15]. Keck NIRSPEC measurements of *vsini* for 19 M to T objects show that T-type objects are generally faster rotators than M-type objects and set a maximum rotation period of 12.5 h for the sample.

The second high amplitude variable found was the T1.5 object 2MASS J21392676+0220226 [59, henceforth 2M2139]. 2M2139 remains the highest amplitude variable brown dwarf known, with a peak-to-peak amplitude in one epoch of 26% in J band [59]. 2M2139 has a variability period of ∼7.7 h and significant evolution of lightcurve features over the timescale of days [59]. Like SIMP 0136, the variability amplitude in $K_S$ is less than that in the shorter wavelength J band.

Finally, at a distance of ∼2 pc, Luhman 16AB are the two closest (and brightest) brown dwarfs known to the earth and were only discovered in 2013 [60]. Luhman 16AB form an L/T transition brown dwarf binary, with T0.5 and L7.5 components [60,61]. Unresolved variability monitoring of both components over 12 nights using the TRAPPIST robotic telescope yielded a detection of quasiperiodic variability with a period of ∼4.9 h and an amplitude of ∼11% in a combined 'I + z' filter extending from 750 to 1100 nm [62]. This variability signal was presumed to be produced by the T0.5 component. Resolved MPG /ESO 2.2 m GROND simultaneous six-band (r'i'z' JHK) photometric monitoring yielded detections of periodic variability in all six bands for Luhman 16B, with amplitudes from 5 to 15% [63] and tentatively in i'z' for Luhman 16A with amplitudes from 1 to 3% [63]. Variability in the A component was later confirmed in [64]. Significant lightcurve evolution even from night to night was reported by both [62] and [63], and found as well in the long-term monitoring of [65,66].

The fact that all three of these highly variable objects are L/T transition objects initially suggested that variability amplitude might be increased along the L/T transition, where thick silicate clouds are breaking up and falling below the photosphere. However, large-scale surveys of many objects were required to determine if this was indeed the case.

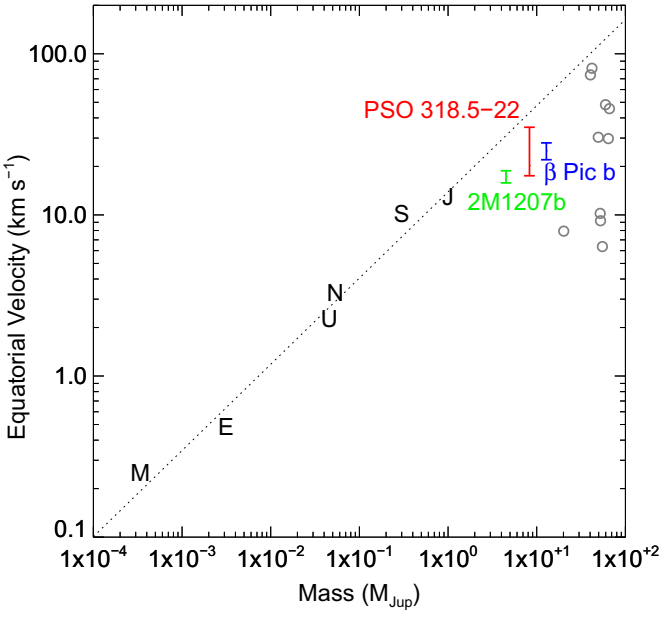


**Figure 3.** Figure from [23], mass vs. equatorial velocity for solar system planets, field brown dwarfs (open circles), and planetary mass objects with measured rotation periods ($\beta$ Pic b, PSO J318.5-22, and 2M12 07b, [18,21–23]).
Notes: The three planetary mass objects with measured rotation periods are all fast rotators compared to solar system planets.

### *2.3. Survey results and constraints on variability frequency and amplitude for L and T brown dwarfs*

While some of the high-amplitude variables described in the last section were discovered serendipitously, large surveys with combined samples of >60 objects were necessary to truly constrain the frequency and amplitude of variability in L and T type brown dwarfs [67–70].

Two large (~60 objects per survey) near-IR ground-based surveys have been completed in the last few years [67,68] using 4-m class telescopes. Both use background stars in the field of view as photometric references to correct for effects of seeing, weather, etc. and are limited to detections of variability with amplitudes greater than 1–2% due to the inherent instability of ground-based observations. Both also robustly detected variability in objects across the full range of L and T spectral types. Radigan et al. [67] found 9 out of 57 of their targets were significantly variable and that all four strong variables discovered (peak-to-peak amplitudes >2%) were L/T transition objects, see Figure 6. Wilson et al. [68] found 14 variables among their 69 targets, and, unlike Radigan et al. [67] found that the frequency of variability in their sample did not change as a function of spectral type. Radigan [71] reanalyzed the data presented in [68] and combined it with her own data from [67]. She failed to recover variability in some of the claimed variables from [68], and, based on her revised classification of variables from [68], she concludes that high amplitude variability does occur more frequently for L/T transition objects, but that high amplitude variables outside of the L/T transition do exist. Nonetheless, both surveys demonstrate that variability is a common feature for both L and T dwarfs.

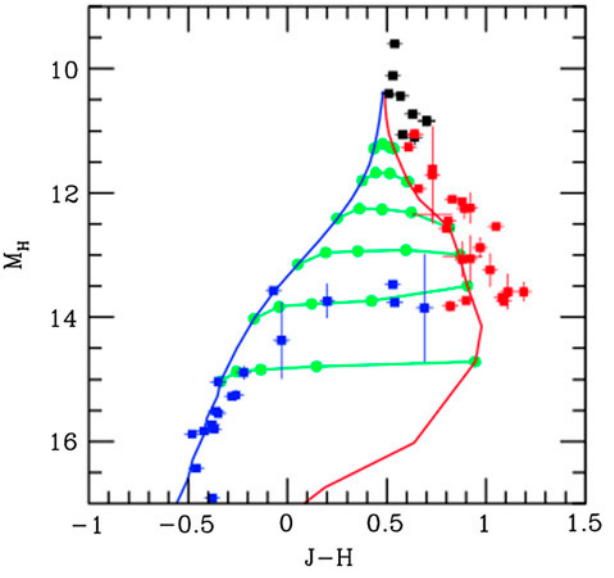


**Figure 4.** Figure from [24], Black points are M stars, red points are L dwarfs, and blue points are T dwarfs. The solid red line is a single-component, completely cloudy model, the solid blue line is a completely clear model, and the solid green lines are patchy cloud models with different values of the cloud sedimentation parameter $f_{sed}$.
Notes: The patchy cloud models best reproduce the notable shift from red to blue colors seen at the L/T spectral type transition.

T-type brown dwarfs may possess particularly high variability amplitudes in the red optical. Based on the observation that the T0.5 object Luhman 16B displays variability amplitudes of 10–20% in the red optical [62,63], Heinze et al. [72] monitored 12 T dwarfs for variability at 0.7–0.95 μm with the Kitt Peak 2.1 m telescope, and found evidence for highly significant variability (>10%) amplitude in two T dwarfs from their sample.

Space-based platforms solve much of the challenge of variability observations, allowing significantly higher photometric precision and stability, and therefore sensitivity down to variability amplitudes of 0.1–0.5%. Large space-based surveys have revealed that low-amplitude brown dwarf variability is quite common. A Spitzer survey of 44 brown dwarfs revealed low amplitude mid-IR variability in >50% of L and T type brown dwarfs [17], see Figure 7. Buenzli et al. [73] find that ∼30% of the L5-T6 objects surveyed in a HST SNAP survey show variability trends. Thus, detecting variability in brown dwarfs is simply a matter of attaining the necessary sensitivity and stability. In fact, using data from the Kepler spacecraft, Gizis et al. [74,75] report a consistent phase and amplitude of 1.4% in optical light over two years of monitoring for the L1 WISEP J190648.47+401106.8!

### *2.4. Detection of variability in late T and early Y brown dwarfs*

While the majority of studies to date focus on L and early/mid T brown dwarfs, the first detections of variability from very cool, late spectral type objects have recently been reported. Rajan et al. [76] surveyed three mid/late T dwarfs and one Y dwarf for variability in J, detecting variability of up to 13% in one epoch for the T8.5 dwarf WISE 0458. However, in followup monitoring two years later, no variability with amplitude >3% was found for

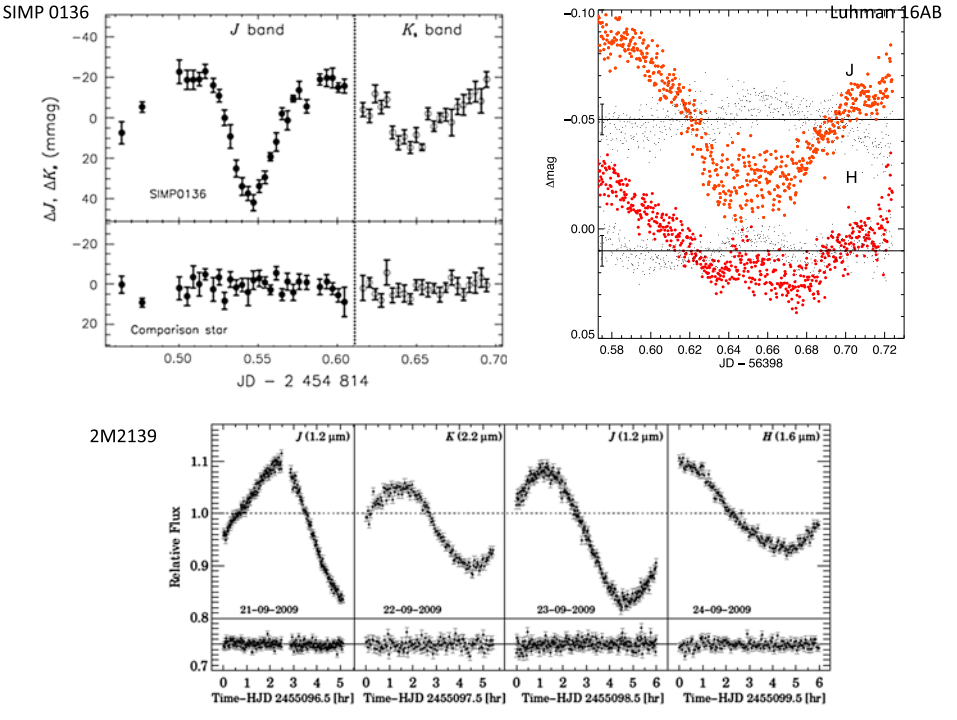


**Figure 5.** Near-IR lightcurves for the first three high amplitude detections of variability, counterclockwise from top left. Top left: Figure from [58]. J and K band lightcurves for the T2.5 SIMP 0136, one of the brightest T dwarfs known. Variability displays a period of ∼2.4 h and a maximum amplitude of ∼50 mmag. Bottom: Figure from [59]. J, H, and K band lightcurves for the T1.5 object 2M2139. This is the highest amplitude variable currently known, with a peak to peak amplitude of ∼26% in this epoch. Top right: Figure from [63]. Combined J and H lightcurves for Luhman 16AB, the two closest brown dwarfs to the earth [60] and an L/T transition brown dwarf binary. Variability up to 15% was observed at these wavelengths, presumed to be primarily from the B component.

this object. Spitzer has yielded the first unambiguous detections of variability in very cool Y brown dwarfs. Cushing et al. [77] detected variability with a period of ∼8.5 h and a semi-amplitude of 3.5% for the spectroscopically confirmed Y-dwarf WISE J140518.39+553421.3. Variability was detected in two epochs separated by 149 days and is well-modeled with a sinusoid. Leggett et al. [78] detected 3% variability at 4.5 μm in the Y0 brown dwarf WISEP J173835.52+273258.9. Recently, Esplin [79] report significant variability for WISE J085510.83+071442.5 henceforth WISE 0855 [80], the coldest brown dwarf known. Esplin [79] detect variability of 3–5% at both 3.6 and 4.5 μm with Spitzer, see Figure 8. Interestingly, WISE 0855 is so cold and so faint that models at all ages predict it should have a mass <10 $M_{Jup}$ – i.e. it is clearly planetary mass. With an effective temperature of $T_{eff} \sim 250K$, WISE 0855 is the coldest atmosphere probed outside our own solar system and the only extrasolar atmosphere studied with an effective temperature comparable (albeit a bit cooler) to that of the Earth. Thus, it is an important precursor regarding variability studies in the next decades of colder directly imaged Jovian planets or even Earthlike planets near or in the habitable zone. The presumed driving factor for this variability would be water vapor clouds in this atmosphere (as opposed to the silicate clouds expected for hotter L type objects), although

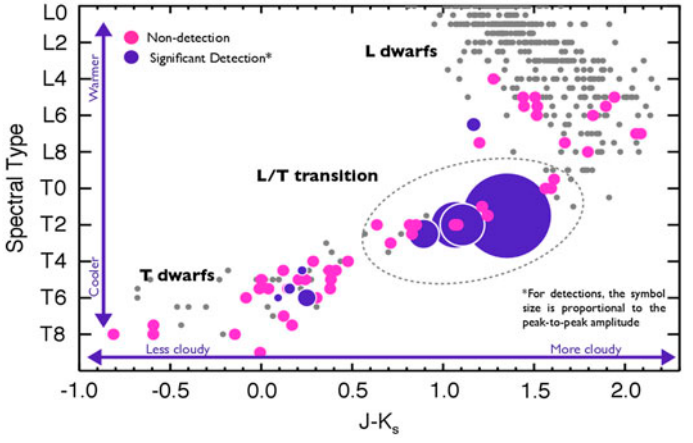


**Figure 6.** Figure from [67], from a variability survey of 62 brown dwarfs.
Notes: Of the 57 brown dwarfs included in their final analysis [67], found that 9 were significantly variable with >99% confidence, with higher variability amplitudes found for L/T transition objects.

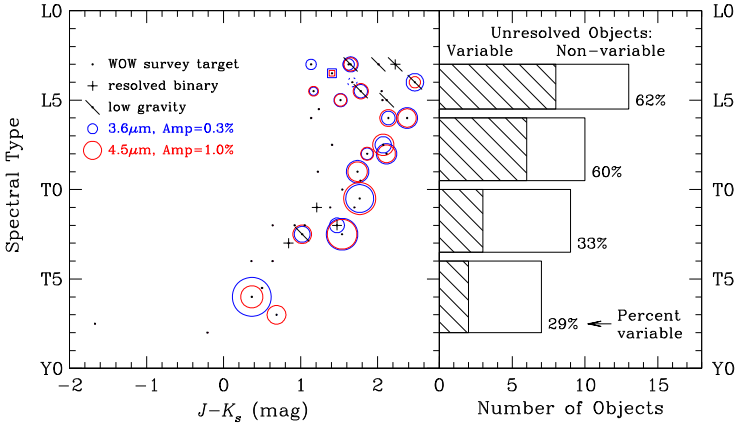


**Figure 7.** Figure from [17], from a Spitzer mid-IR variability survey of 44 brown dwarfs. Metchev et al. [17] find ubiquitous variability at low amplitudes as well as a tentative association (92% confidence) between low surface gravity and high-amplitude variability among L3-L5.5 dwarfs. Based on these results, variability up to the few percent level appears to be a common feature for L and T brown dwarfs

[79] find that in this case, the relatively small amplitudes of variability would imply very small differences in cloud coverage between hemispheres.

### *2.5. Multi-wavelength/spectroscopic variability monitoring*

Monitoring brown dwarfs simultaneously at multiple wavelengths opens up a wealth of characterization possibilities. Differences between amplitudes and phases at different wavelengths allow robust tests of various mechanisms for driving variability – mechanisms that range from inhomogenous cloud cover [81], temperature perturbations [27], and thermochemical instabilities [28,29].

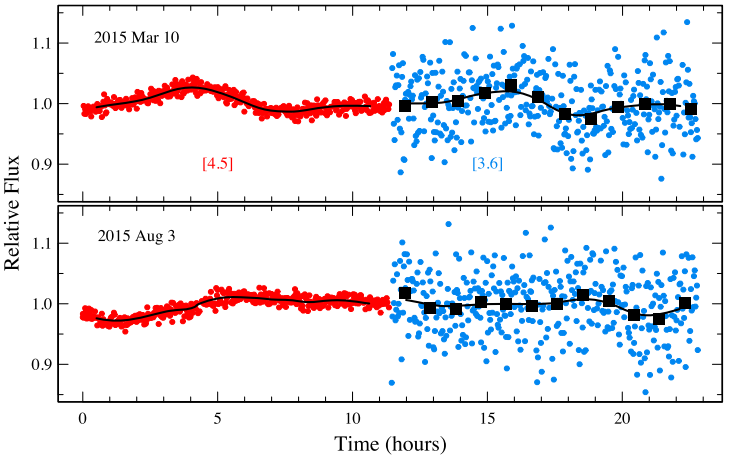


**Figure 8.** Figure from [79], lightcurves for WISE 0855, the coldest brown dwarf known, with clearly planetary mass estimates.
Note: Esplin et al. [79] find 3–5% mid-IR variability for this object at multiple epochs.

The first few variable brown dwarfs studied simultaneously or near-simultaneously in multiple wavelengths displayed varying amplitudes in different wavelengths, but generally the same phase at all wavelengths – for instance, SIMP 0136 and 2M 2139 both have smaller $K_S$ variability amplitudes than J, but the phases of the lightcurves in these different bands match up. In contrast, Buenzli et al. [82] found that while variability for the T6.5 brown dwarf 2MASSJ22282889-431026 is well modeled as a sinusoid, the phase of the sinusoid varies significantly with band. In fact, the phase lag between bands increases with decreasing pressure level, aka higher altitude in the atmosphere of this object [82]. This implies that the structures causing the variability must differ in position in higher vs. lower pressure layers of the atmosphere. Biller et al. [63] found a similar trend for the T0.5 dwarf Luhman 16B, with i' and z' anticorrelated with J and H lightcurves, and $K_S$ showing a significant phase lag relative to H. Recently, Yang et al. [83] reported phase shifts between near-IR and mid-IR lightcurves for all four objects for which they obtained simultaneous HST and Spitzer monitoring, suggesting that such shifts are common, and show diversity in inhomogeneous structures between higher altitudes (probed by the mid-IR) and lower altitudes (probed by the near-IR)

For variable brown dwarfs which display correlated variability between wavelengths, spectroscopic variability monitoring has yielded valuable constraints on the source of the variability and the cloud structure of these atmospheres. By fitting combined spectra of two or more 1-D cloudy models with varying cloud properties (or cloudy and clear models) to spectra across the time series, one can find which combination of models and cloud filling fraction best describes the observed spectroscopic lightcurves. It is important to note that in most cases (with the exception of Ref. [84]), this has not been done in an internally consistent manner – the 1-D models being combined do not share the same pressure–density profile. However, such model-fitting can still yield insight into the cloud features of these objects. Marley et al. [24] suggested that completely depleted holes in cloud cover could develop across the L/T transition, allowing a view into the hotter, clear photosphere of the object. The reality appears to not be so extreme – multiwavelength lightcurves of

the three highly variable L/T transition objects described above (SIMP 0136, 2M 2139, and Luhman 16B) are all better fit by the combination of multiple thin and thick cloud species as opposed to combinations of cloudy and clear models [59,64,81,85].

Not all variability is produced by patchy clouds relatively low in the atmosphere – for objects outside the L/T transition, especially earlier L type objects, variability may be caused by spatially varying high-altitude haze layers above the thick condensate cloud decks expected for L type objects. [86], found low amplitude variability in HST observations of two mid-L brown dwarfs. Unlike previous HST variability monitoring of L/T transition objects [81,85] that found that amplitude of variability at the water absorption feature seen at 1.4 $\mu$m is about half of that seen at other wavelengths, the variability amplitude at 1.4 $\mu$m for the L dwarfs studied by [86] was comparable to that seen at other wavelengths (see Figure 9). Therefore, the condensates responsible for the variability must be located at very low pressure, high and dry parts of the atmosphere where water opacity is negligible. Hence, the variability for these two objects (and likely other early-mid L objects) is likely driven by hazes at high altitudes.

Apart from the 1.4 $\mu$m water absorption feature, another obvious feature in which to search for spectroscopic variability is the 0.99 $\mu$m FeH feature. FeH absorption vanishes in mid to late L dwarfs, but re-emerges in early to mid T dwarfs [16,87]. The strength of this feature may indicate whether Fe is sequestered in clouds or not – for the cloudy L dwarfs, iron is primarily in condensate clouds, weakening the FeH gas feature. For late L dwarfs, the feature weakens further, as these Fe clouds sink beneath the photosphere. The re-emergence of this feature in early T dwarfs in particular was interpreted as holes developing in the clouds of these objects, allowing deeper, clear regions to be probed – regions where Fe is not sequestered in clouds, but is still present in gases like FeH. Thus, if this interpretation is correct, variability should be seen in this spectral line as cloudy and clear regions pass across the face of this object. Cushing et al. [88] showed as well that a combination of clouds of different thickness could also produce an increase in FeH absorption for early T objects. Nonetheless, Buenzli et al. [64] do not see significant FeH variability relative to other wavelengths for either component of the L/T transition binary Luhman 16AB.

The majority of models of brown dwarfs and young giant exoplanets require condensates to describe the L/T and T/Y transitions [16,24,84,89,90], and the variability community has correspondingly seized upon the condensates in these models to explain variability observed to date [64,81,85]. However, new, cloud-free models have recently become available [28,29] which produce the observed changes with spectral type as the result of thermochemical instabilities in the $CO/CH_4$ transition in the case of the L/T boundary and the $N_2/NH_3$ transition in the case of the T/Y boundary. Tremblin et al. [29] suggest that variability in these objects may be due to surface inhomogeneities due to differing CO abundances or temperature. However, abundance differences at different surface points should be traceable through variability within particular spectral lines – e.g. the methane absorption feature at 1.6 $\mu$m. To date, variable L/T transition objects have not displayed significantly higher or lower variability amplitudes in methane absorption compared to other wavelengths [85], suggesting that surface composition variations are not the culprit in producing variability.

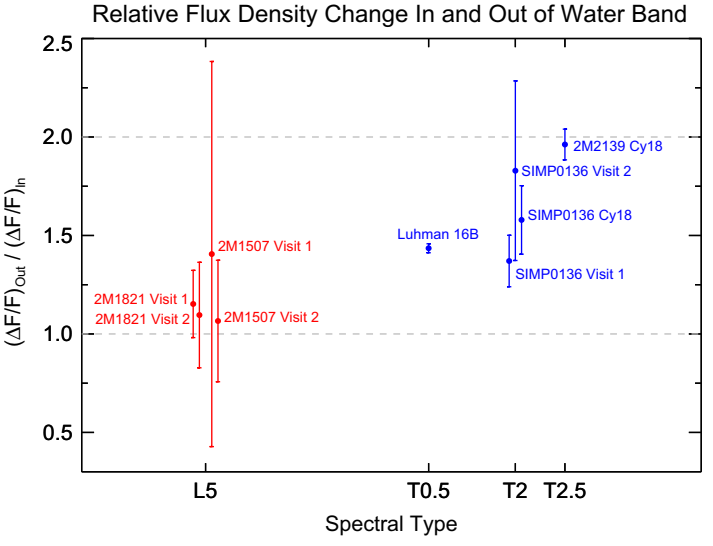


**Figure 9.** Figure from [86]. The amplitude of variability in the 1.4 μm water absorption feature in variable mid L dwarfs is similar to that in other bands; the amplitude of variability in this feature for later L/T transition objects is half of that seen at other wavelengths.
Notes: This implies that the condensates responsible for variability in the early-mid L objects must be located at very low pressure, high and dry parts of the atmosphere, with negligible water opacity.

### *2.6. Surface mapping techniques*

As previously noted, variability requires inhomogeneous surface features on the variable objects. Measuring variability in turn allows us to probe the shape and extent of these surface features.

Kostov and Apai [91] built Stratos, a PCA-based code which models surface features as elliptical spots drawn from two different model atmospheres (e.g. clear vs. cloudy, thin vs. thick clouds, etc). While Stratos predicts the number of such surface features necessary to describe observed lightcurve structure, its outputs are highly degenerate (partly due to the unknown inclination to the line of sight of the brown dwarf being studied). Apai et al. [81] applied Stratos to HST WFC3 lightcurves of the two highly variable brown dwarfs 2M2139 and SIMP 0136. While multiple degenerate solutions fit the lightcurve (see Figure 10), they found that at least 3 elliptical spots on the surface of each brown dwarf were necessary to describe the lightcurves, and that clear + cloudy models could not produce the observed features (which would predict anti-correlated variability between J and $K_S$). Instead, the observed variability was best fit by a combination of low-temperature thick clouds and thin warm clouds, see Figure 11.

Karalidi et al. [92] built Aeolus, a Markov-Chain Monte Carlo code that models surface features as elliptical spots with semimajor axes parallel to the equator, then fits for the number, contrasts, and positions of spots necessary to produce a specific lightcurve, assuming a set value for limb darkening and an equator-on inclination. Future versions of Aeolus will also fit inclination and limb darkening as free parameters. Karalidi et al. [92] verified this code using a unique HST observation of Jupiter and were able to retrieve all the major features observed in Jupiter's atmosphere. Karalidi et al. [92] also applied Aeolus to the variable brown dwarfs 2M 2139 and SIMP 0136 – both objects required three spots

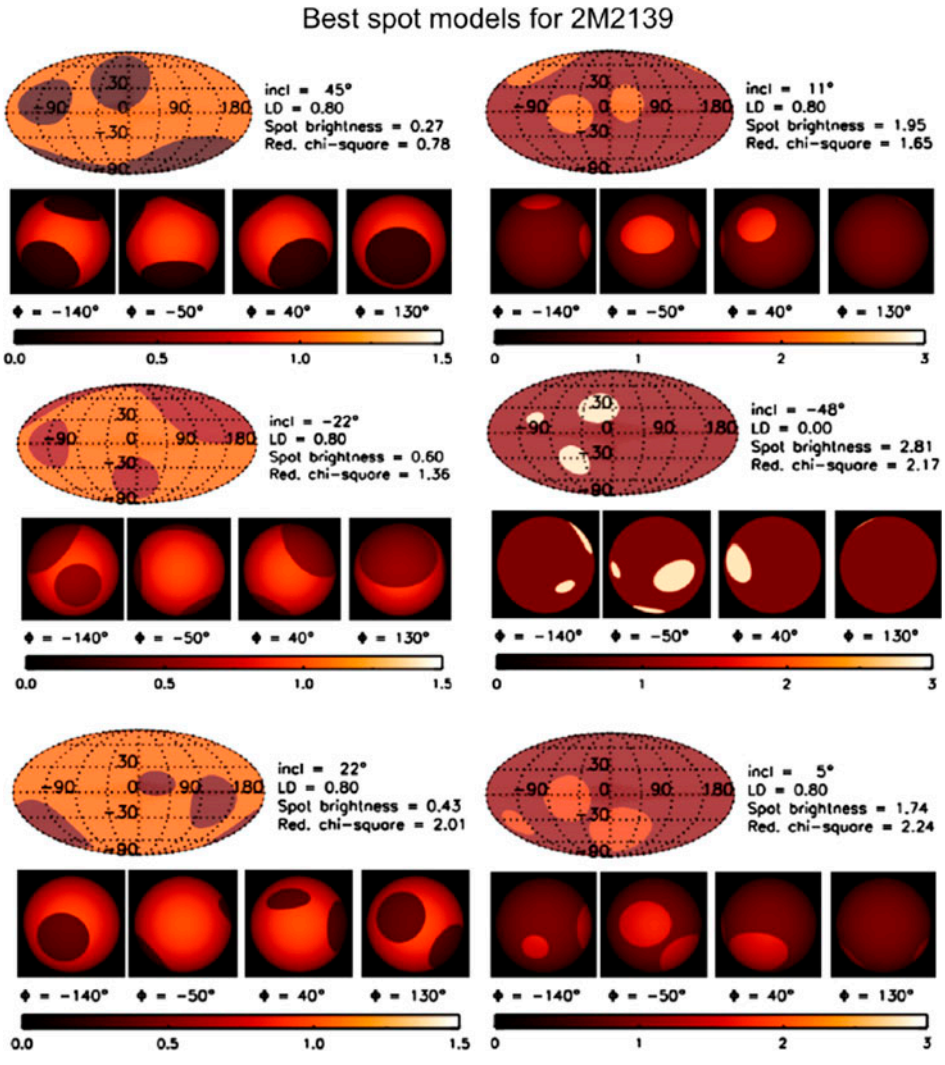


**Figure 10.** Suite of Stratos maps for 2M2139, from [81].
Notes: While a variety of maps with different values of inclination, hot vs. cold spots, etc. can fit the observed variability, all fitting maps required three or more spots to do so.

with a coverage of ∼20% of the surface to model the observed variability. Karalidi et al. [93] applied an upgraded version of Aeolus (including inclination as an additional parameter to fit) to both components of the brown dwarf binary Luhman 16AB (see Figure 12), creating the first surface map for the A component and finding spot surface coverage of ∼20–40% depending on the epoch for both components.

The technique of Doppler Imaging can also be used to directly probe the surfaces of variable brown dwarfs. Briefly, Doppler Imaging uses the Doppler shift of spectral features to reconstruct surface features of the object. To understand how this technique works, consider a rotating star/brown dwarf with one large spot. As the spot rotates across the limb and into visibility, it will be blue-shifted. As it passes across the face of the object, it will show no Doppler shift. As it rotates across the limb and out of view, it will be red-shifted. If

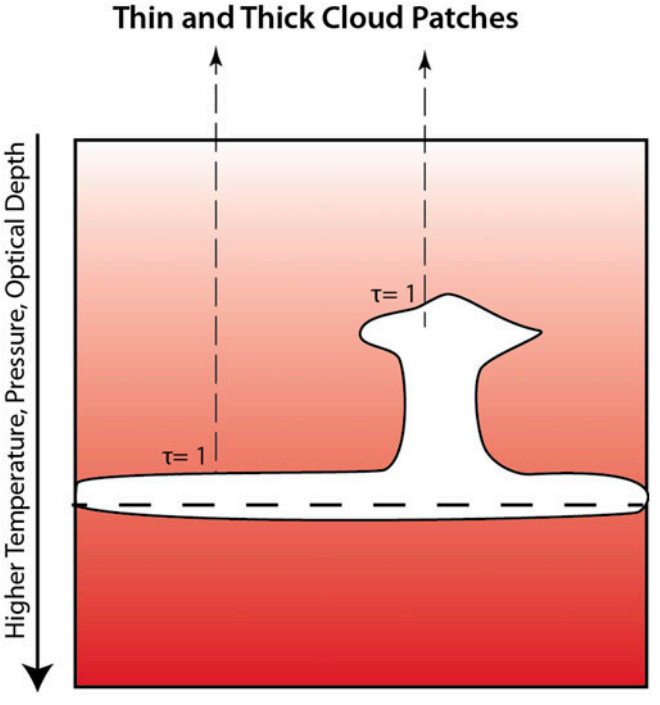


**Figure 11.** Figure from [81]. Variability due to inhomogeneous clouds for L/T transition brown dwarfs is best modeled by a combination of thin clouds at higher temperatures and thicker regions of clouds extending up to lower pressure, cooler parts of the atmosphere.

the spot is located on the equator, it will appear to rotate more quickly than if it is located closer to the poles. Thus, from a high S/N, high resolution ($R > 30000$) combined line profile, it is possible to reconstruct surface features on such an object by measuring Doppler shifts within this line profile. This technique has previously been used to reconstruct surface spot features for low mass stars [95–97], but has been applied to brown dwarfs only recently. [94] produced the very first Doppler image of a brown dwarf (see Figure 13) for the closest brown dwarf to the Earth, Luhman 16B [94], using the high-resolution spectrograph CRIRES at the VLT in K band ($\sim$2.2 $\mu$m). Luhman 16B is 10–15% variable in $K_S$ [63] – the surface features seen in the Doppler map are consistent with this variability amplitude. While an object as bright as Luhman 16B could actually be mapped with a 4-m class telescope with a spectrograph such as ishell on the IRTF [98], this technique could also be applied to a handful of fainter brown dwarfs using a high resolution spectrograph such as CRIRES (currently being upgraded but expected back in service in 2018) with an 8-m class telescope. Extremely large telescopes (ELT) will open up a wider cohort of brown dwarfs to Doppler imaging.

## 3. Current state of the art for exoplanet analogs and exoplanet companions

As we have seen, variability is robustly observed in field brown dwarfs. Thus, variability may also be expected for young extrasolar planets, which share similar $T_{\rm eff}$ and L and T spectral types, but have lower surface gravities. Indeed, the spectrum of the young planet HR 8799b

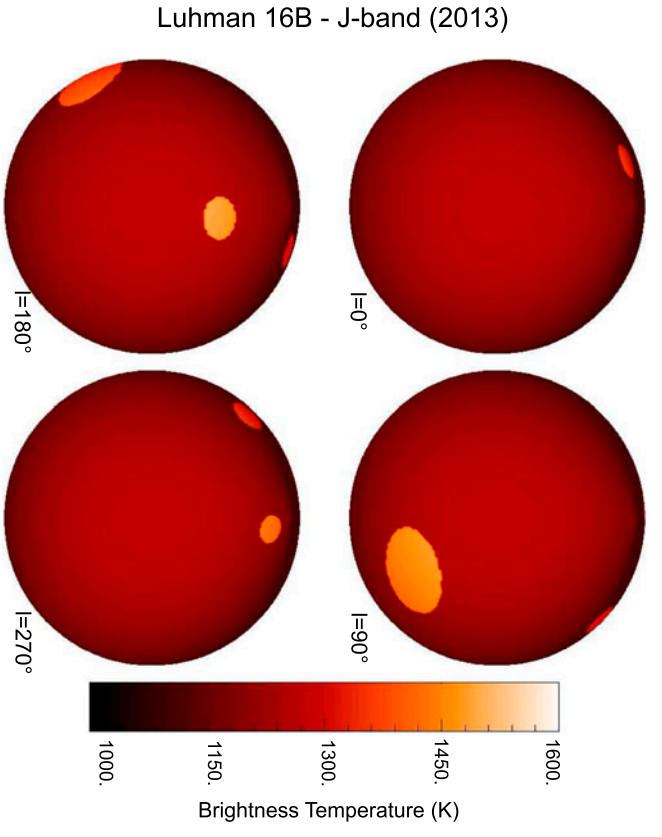


**Figure 12.** J-band Aeolus map for Luhman 16B from [93].
Notes: Karalidi et al. [93] find that the best fit requires three spots and retrieve an inclination of $26^\circ \pm 8^\circ$, agreeing with the measured inclination of $<30^\circ$ from [94].

is nearly identical to that of the most variable brown dwarf known, 2M 2139 and [17] found a tentative association (92% confidence) between low surface gravity and high-amplitude variability among the 8 low-surface gravity, young L3-L5.5 dwarfs in their sample.

Young, directly imaged exoplanet companions such as HR 8799b share similar temperatures and likely compositions with older field brown dwarfs. However, the key difference between these two categories of objects is the lower surface gravities of the exoplanet companions. There are two main reasons for this: (1) young objects are likely somewhat larger than older objects since they have not fully contracted yet and (2) due to degeneracy pressure in their cores, objects with quite a wide range of masses (roughly 1–100 $M_{Jup}$) are similar in size to Jupiter, with younger, low surface gravity objects having radii of up to 1.5–1.6 $R_{Jup}$ s [18]. Thus, for young, low mass (<25 $M_{Jup}$) objects, less mass is packed into the same volume compared to older, more massive field brown dwarfs. As has been already noted, the low surface gravity in younger and lower mass objects significantly affects the spectra of these objects (and also the $T_{eff}$) at which these objects transition between spectral types [14]. While only a handful of exoplanet companions are amenable to variability searches, a wider class of 'exoplanet analogues' can be defined with similar spectral types and surface gravities as young exoplanet companions. These include bonafide free-floating

planetary mass objects such as PSO J318.5-22 [99] as well as somewhat higher mass (<25 $M_{Jup}$), young objects such as WISEP J004701.06+680352.1 (henceforth W0047), a ~20 $M_{Jup}$, very red AB Dor (~125 Myr) moving group member [75,100]. These two objects have spectra that are nearly identical to the outer two HR 8799 planets [3].

### 3.1. First detections

Two initial detections of quasiperiodic variability in young, clearly planetary mass objects with L/T spectral types have been reported in the last year (see Figure 14). For clarity, we note that there are a handful of non-periodic detections for very young M-type objects [32], but these are accreting objects, with a very different mechanism for driving variability.

PSO J318.5-22 is an ~8 $M_{Jup}$ member of the 23 ± 3 Myr $\beta$ Pic moving group [23,99]. PSO J318.5-22 is intermediate in mass between 51 Eri b and $\beta$ Pic b, the two known exoplanet companions in the $\beta$ Pic moving group. Biller et al. [22] report variability amplitudes with the SofI imager at the 3.6 m NTT from 7 to 10% in $J_S$ at two separate epochs over 3–5 h observations and marginally detect a variability trend of up to 3% over a 3 h $K_S$ observation. They hence constrain the rotational period of this object to >5 h. This is also the highest amplitude variability detection among L dwarfs surveyed at high photometric precision (<3%). Subsequently Allers et al. [23], measured a *vsini* of $17.5^{+2.3}_{-2.8}$ km $s^{-1}$ for PSO J318.5-22. Making reasonable assumptions regarding the size of this object and combining with the photometric variability data from [22], Allers et al. [23] thus constrain the inclination of PSO J318.5-22 to >29° and its rotational period to 5–10.2 h.

2MASSWJ1207334-393254b (henceforth 2M1207b) was the first planetary mass companion to be directly imaged [101,102], in this case around a 25–30 $M_{Jup}$ brown dwarf as opposed to a main-sequence star. 2M1207b is a member of the TW Hya association (~8 Myr) age with an estimated mass of 2–5 $M_{Jup}$. Using the HST Wide Field Camera 3, Zhou et al. [21] observed in two separate bands and with two telescope roll angles. To overcome the contrast between the companion and its primary, they used point-spread function fitting photometry, finding variability with an amplitude of 1.36% in F125W and 0.78% in F160W. This variability was well-fit with a sine curve with a period of $10.7^{+1.2}_{-0.6}$ h and with the same phase in both bands.

Recently, variability was also reported for WISEP J004701.06+680352.1 (henceforth W0047), a ~20 $M_{Jup}$, very red AB Dor (~125 Myr) moving group member [75,100,103]. Like PSO J318.5-22, W0047 has an extremely high variability amplitude for an L dwarf (8%), suggesting that young, low-surface gravity late-Ls may be considerably more variable than their older, high-surface gravity counterparts.

These objects are clear analogs in colors and spectral properties to exoplanet companions to stars such as the HR 8799 planets and $\beta$ Pic b. In particular, Bonnefoy et al. [3] find that PSO J318.5-22 shares very similar photometry with the closest in of the HR8799 planets, HR 8799e. Thus, these results suggest that exoplanet companions to main sequence stars are likely also variable.

### 3.2. Ongoing surveys of variability in free-floating planetary mass objects

While instruments such as Gemini Planet Imager (GPI, Ref. [104]) and SPHERE [105] achieve contrasts suitable to enable variability studies for a handful of exoplanet companions, it is currently prohibitively difficult to study variability for a statistically significant sample of

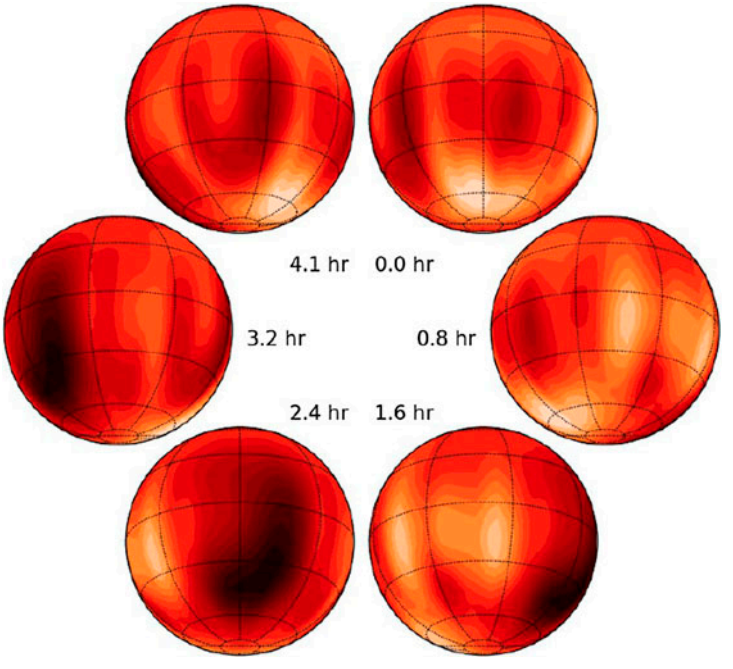


**Figure 13.** Figure from [94], Doppler map of the nearby brown dwarf Luhman 16B.
Note: The surface features observed are consistent with the observed near-IR variability.

directly imaged planets within 1″ of their star. However, we can circumvent the contrast issue and probe variability for young 3–25 $M_{Jup}$ objects by observing widely (>1″) separated companions and isolated very low mass young brown dwarfs and planetary mass objects.

Vos, Biller et al. in prep are currently conducting the first statistically significant survey of weather patterns on young exoplanet analogs (free-floating planetary mass objects as well as <25 $M_{Jup}$, young, low-surface gravity brown dwarfs) using the Son of Isaac (henceforth SofI) imager at the La Silla Observatory New Technology Telescope (henceforth NTT). We have obtained to date $J_S$-band photometric variability monitoring observations for a sample of 24 young L and T type objects with masses <25 $M_{Jup}$, drawn from the samples of [106–109]. This survey has already yielded the first detection of variability in a free-floating L/T transition planetary mass object [22], described above, as well as lower amplitude detections in three additional objects (Vos et al. in prep).

### *3.3. Searches for variability in high-contrast companions*

Searches for variability in exoplanet companions have only recently become possible with the advent of next generation planet imagers such as GPI and SPHERE. Planets which previously required ∼1 h of on-sky time to image can be detected even in 5–10 min of data from these imagers! Thus, multiple groups are pursuing variability studies for bright exoplanet companions such as $\beta$ Pic b and HR8799b.

Only one variability monitoring result for exoplanet companions to stars has been published to date, likely because these observations are extremely challenging! In relatively

PSO J318.5-22, Biller et al. 2015

2M1207b, Zhou et al. 2016

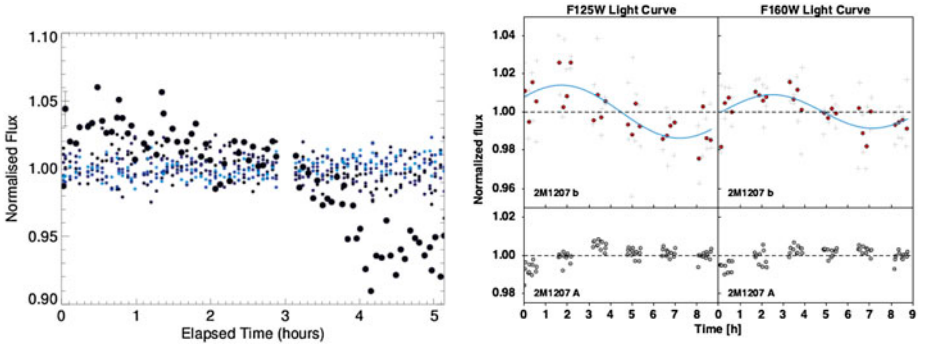


W0047, Lew et al. 2016

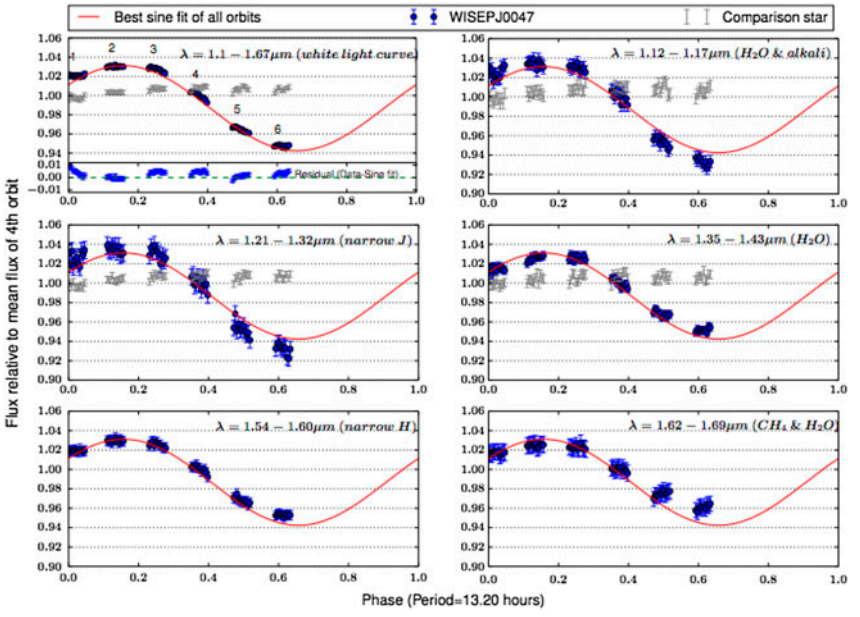


**Figure 14.** Near-IR lightcurves for the first three detections of variability in young planetary mass objects/very low mass brown dwarfs. Top left: Figure from [22]. $J_S$ lightcurves for PSO J318.5-22, an $\sim$8 $M_{Jup}$ member of the 23 $\pm$ 3 Myr $\beta$ Pic moving group [23,99]. Top right: Figure from [21]. HST lightcurves for 2M1207b, a $\sim$8 Myr TW Hya association member and the first planetary mass companion to be directly imaged [101,102], in this case around a 25–30 $M_{Jup}$ brown dwarf. Bottom: Figure from [103]. HST lightcurves for W0047, a $\sim$20 $M_{Jup}$, $\sim$125 Myr member of the AB Dor moving group.

short SPHERE observations of the HR 8799 planetary system, Apai et al. [110] show proof-of-concept for variability monitoring using an extreme AO system with artificial photometric references provided by using the deformable mirror to induce satellite spots on the image. This study was limited by the short observation length at each of the four epochs of data. Nonetheless, using satellite spot-modulated artificial planet-injection based photometry with a PCA speckle removal algorithm led to a 3$\times$ gain in photometry accuracy over aperture photometry.

### 3.4. Future prospects

It is important to constrain variability of planetary mass objects (both free-floating and companions) now, as significant variability in exoplanet companions will lead to even more exciting followup possibilities with future ELT instruments. For instance, Crossfield et al. [94] used VLT CRIRES to produce a surface map of the highly variable L/T transition brown dwarf Luhman 16B with the doppler imaging technique (see Figure 13). If young planets such as $\beta$ Pic b are similarly variable in the L′ bandpass, the high resolution spectroscopy mode anticipated for the E-ELT mid-IR instrument METIS will enable similar mapping of exoplanet surfaces (see e.g. [18]).

In the next couple of years, JWST will be transformative for searches for variability in young, bright exoplanet companions such as HR 8799bc and $\beta$ Pic b. As noted previously, space-based searches avoid the stability issues endemic from the ground, which limit sensitivity to variability amplitudes $\geq$1%. However, HST does not possess appropriate coronagraphs to enable variability searches for these objects. Along with the exquisite stability only available from space, JWST possesses a suite of coronagraphs suitable for variability studies of relatively wide (>0.5″) separation exoplanet companions.

To date, no directly imaged exoplanet and few brown dwarfs have been characterized at wavelengths longer than 5 $\mu$m. This is because current facilities are ground based and thus suffer from the very high sky background at these long wavelengths (since the blackbody peak for the Earth's atmosphere occurs at a wavelength of $\sim$10 $\mu$m). The JWST MIRI instrument will enable high-sensitivity observations at these wavelengths, both for field objects and also for companions using four-quadrant phase masks at 10.65, 11.4 and 15.5 $\mu$m, and a Lyot coronograph at 23 $\mu$m [111]. The four-quadrant phase masks have inner working angles at approximately $\lambda/D$, limiting studies to companions at separations greater than 0.35–0.5″. Nonetheless, this will enable long wavelength photometry and variability monitoring of much of the cohort of directly-imaged exoplanet companions.

The high quality spectra and photometry of brown dwarfs and giant exoplanets from JWST will enable variability-focused atmospheric retrieval studies for these objects. Instead of the dominant forward modeling approach used where models are run independently and then fit to observations, the retrieval method utilizes a Bayesian framework (Markov-chain Monte-Carlo, nested sampling) to represent a set of data and associated errors and infer posterior distributions on each free parameter considered in the models. This method has already yielded insights into the atmospheric temperatures and cloud profiles of brown dwarfs [112–114] as well as transiting exoplanets [115,116]. Time-resolved near- to mid-IR spectroscopy from JWST will allow this technique to be extended to the variability case as well, allowing us to pinpoint exactly what is changing in the cloud or temperature profiles of these objects as a function of time.

In the more distant future with the ELTs as well as giant space telescopes such as LUVOIR, variability studies will be a key probe of colder giant and eventually super-Earth and Earth mass planet atmospheres. Disc-averaged variability studies of Jupiter and Neptune [92,117,118] provide a preview of what we may eventually find for cooler atmospheres outside our own solar system. Here, the variability mechanism is clearly clouds – and at low temperatures with multiple cloud components (ammonia, ammonium hydrosulfide, water, etc.), such objects have optical variability with amplitudes >1% and rapidly changing variability profiles.

## 4. Modeling approaches – dealing with inhomogeneous surface features

Variability in both brown dwarfs and planetary mass objects implies inhomogenous surface features (whether due to clouds or other mechanisms) that cannot be accounted for with solely 1-D models. However, most state of the art models are completely 1-dimensional – see review by [119]. Most observers have thus interpreted brown dwarf and planetary mass object lightcurves using unphysical combinations of multiple 1-D models (e.g. [59,81]), for lack of available 2-D models. However, modelers are beginning to account for 2-D cloud (and other) structures in their models.

Specifically to address the sources of observed variability, Morley et al. [84] calculate a combined cloudy and clear model (50% cloudy overall, but with a more-cloudy and less-cloudy hemisphere) considering two columns but a combined temperature/pressure profile. They utilized silicate clouds for L-type and L/T transition objects as well as cloud species expected to condense at cooler temperatures for later Ts and Y dwarfs [90,120]. Morley et al. [84] also modeled the case of hot-spot driven variability, simulating a hot spot covering 5% of the surface of the object, with heating at different pressure levels (0.1, 0.3, 1, 3, 10, and 30 bar) in the atmosphere as the source of the hot spot. Both mechanisms produce variability, but with considerably different spectral and photometric properties. They conclude that patchy clouds drive the highest amplitude variability within spectral window while hot spots produce larger variability within absorption features. The details of the spectral dependence depends on the cloud species or depth of the hot spot – but should be identifiable by spectroscopic variability monitoring across a wide wavelength regime.

Robinson and Marley [27] also investigate temperature fluctations as a potential source of the observed variability. They find that for certain periodic perturbations, they can reproduce phase shifts similar to those found in the T6 2M2228 [82]. However, the presence of temperature fluctuations does not preclude cloud based variability, nor vice versa – in fact [27] note there is much interplay between these mechanisms, e.g. in the case where a cold spot promotes cloud formation or a hot spot inhibits it. Stark et al. [121] consider an alternate method of producing inhomogeneous cloud cover without accompanying temperature differences, where charge in these atmospheres can accumulate on dust particles, eventually breaking up smaller particles.

Simply considering a 2-D atmosphere with multiple cloud species is not sufficient to fully model variability for these atmospheres, however; as noted previously, brown dwarfs are rapid rotators and at least some young planetary mass objects are as well [18,21–23]. This rapid rotation has strong ramifications for the cloud structure. Showman et al. [122] developed three-dimensional global, anelastic numerical simulations of convection in the interior of brown dwarfs and found that rotation significantly affected the convective properties of these objects, producing sizable temperature variations across the surface of the object. Zhang and Showman [123] investigated the global atmospheric dynamics of brown dwarfs using a shallow-water model. Depending on rotation rate and atmospheric parameters, they found two primary regimes of surface features: (1) jet-dominated, where strong energy injection and weak dissipation produces large-scale east–west jet streams (similar to what is observed for Jupiter) and (2) vortex-dominated, where weak energy injection and strong dissipation produces a surface covered by transient vortices. Using time variability of face-on geopotential anomaly as a proxy for infrared lightcurves, Zhang

and Showman [123] find that both cases can produce the quasiperiodic variability observed in brown dwarfs, although note that the vortex-dominated case is more likely for brown dwarfs. Neither [122] or [123] incorporate radiative transfer into their models, so a direct comparison to observed lightcurves is not possible. Full 3-D Global Circulation Models (henceforth GCM) with radiative transfer incorporated have yet to be developed for brown dwarfs or giant planets, although such models have been applied to solar system gas giants. Mayne et al. [124] have adapted the UK Met Office Unified Model for hot Jupiter planets and plan to adapt it as well for brown dwarfs and giant non-irradiated exoplanets.

## 5. Conclusions

To summarize the current state of the art of our understanding of variability in L/T/Y field brown dwarfs as well as their low surface gravity young counterparts:

- Variability is common in L and T field brown dwarfs. Ground -based surveys find that >10% of objects have variability >1% in the near-IR [67,68,71]. Space-based surveys (which probe down to much smaller variability amplitudes) find >50% of these objects have variability down to the 0.1–0.5% level [17].
- The current dominant theory as to the source of this variability is inhomogeneous cloud cover – i.e. combination of multiple cloud species, in particular thinner and thicker cloud regions in these atmospheres [81]. However, temperature profile variations [27] and thermochemical instabilities [28,29] have also been proposed as mechanisms for driving variability.
- Based on their spectral types and colors, young giant planets and low mass brown dwarfs should also be variable. However, these objects have significantly redder colors than old field objects, likely due to their considerably lower surface gravities.
- The first detections of variability in young, low-surface gravity objects have all been in L type objects (as opposed to L/T transition objects [21,22,103]). PSO J318.5-22 and W0047 display the highest variability amplitudes found in *any* L type object [22,103].
- For both old and young objects, spectroscopic variability monitoring and spectral mapping/doppler imaging techniques offer valuable insights into the atmospheres of these objects. From spectroscopic variability monitoring, variable L/T transition brown dwarfs like SIMP0136 and 2M 2139 are best described by a combination of thin and thick cloud patches, as opposed to cloudy and clear patches [81]. Doppler imaging has recently yielded the first surface map of any brown dwarf [94].
- Next generation telescopes and instruments, such as METIS at the E-ELT and, in the shorter term, the various instruments of JWST, will enable similar characterization of exoplanet atmospheres. For instance, if the directly imaged planet $\beta$ Pic b has significant variability at L', METIS will be able to produce a Doppler map of its surface.

The first surveys of variability in young free-floating exoplanet analogs as well as the first searches for variability in exoplanet companions are currently underway. In the next few years, these studies will provide a key probe of cloud properties in the atmospheres of both exoplanet companions and similar free-floating objects. This is already the case for field L and T brown dwarfs, where variability studies suggest that top-of-atmosphere inhomogeneity is a dominant feature of these atmospheres.

## Disclosure statement

No potential conflict of interest was reported by the author.

## Funding

This work was supported by STFC [grant number ST/M001229/1].

## ORCID

*Beth Biller* http://orcid.org/0000-0003-4614-7035

## References

[1] Burgasser AJ. The SpeX Prism Library: 1000+ low-resolution, near-infrared spectra of ultracool M, L, T and Y dwarfs. In: Astronomical society of India conference series (Astronomical society of India conference series; Vol. 11:7); 2013 Oct 14–17; Lyon, France.
[2] Allers KN, Liu MC. A near-infrared spectroscopic study of young field ultracool dwarfs. Astrophys J. 2013 Aug;772:79.
[3] Bonnefoy M, Zurlo A, Baudino JL, et al. First light of the VLT planet finder SPHERE. IV. Physical and chemical properties of the planets around HR8799. Astron Astrophys. 2016 Mar;587:A58.
[4] Zurlo A, Vigan A, Galicher R, et al. First light of the VLT planet finder SPHERE. III. New pectrophotometry and astrometry of the HR 8799 exoplanetary system. Astron Astrophys. 2016 Mar;587:A57.
[5] Bonnefoy M, Marleau GD, Galicher R, et al. Physical and orbital properties of $\beta$ Pictoris b. Astron Astrophys. 2014 Jul;567:L9.
[6] Ingraham P, Marley MS, Saumon D, et al. Gemini Planet Imager spectroscopy of the HR 8799 planets c and d. Astrophys J Lett. 2014 Oct;794:L15.
[7] Chilcote J, Barman T, Fitzgerald MP, et al. The first H-band spectrum of the giant planet $\beta$ Pictoris b. Astrophys J Lett. 2015 Jan;798:L3.
[8] De Rosa RJ, Rameau J, Patience J, et al. Spectroscopic characterization of HD 95086 b with the Gemini Planet Imager. Astrophys J. 2016 Jun;824:121.
[9] Macintosh B, Graham JR, Barman T, et al. Discovery and spectroscopy of the young jovian planet 51 Eri b with the Gemini Planet Imager. Science. 2015 Oct;350:64–67.
[10] Wagner K, Apai D, Kasper M, et al. Direct imaging discovery of a Jovian exoplanet within a triple-star system. Science. 2016 Aug;353:673–678.
[11] Kirkpatrick JD. New spectral types L and T. Ann Rev Astron Astrophys. 2005 Sep;43:195–245.
[12] Cushing MC, Kirkpatrick JD, Gelino CR, et al. The discovery of Y dwarfs using data from the wide-field infrared survey explorer (WISE). Astrophys J. 2011 Dec;743:50.
[13] Kirkpatrick JD, Gelino CR, Cushing MC, et al. Further defining spectral type 'y' and exploring the low-mass end of the field brown dwarf mass function. Astrophys J. 2012 Jul;753:156.
[14] Barman TS, Macintosh B, Konopacky QM, et al. Clouds and chemistry in the atmosphere of extrasolar planet HR8799b. Astrophys J. 2011 May;733:65.
[15] Zapatero Osorio MR, Martín EL, Bouy H, et al. Spectroscopic rotational velocities of brown dwarfs. Astrophys J. 2006 Aug;647:1405–1412.
[16] Burrows A, Sudarsky D, Lunine JI. Beyond the T dwarfs: theoretical spectra, colors, and detectability of the coolest brown dwarfs. Astrophys J. 2003 Oct;596:587–596.
[17] Metchev SA, Heinze A, Apai D, et al. Weather on other worlds. II. Survey results: spots are ubiquitous on L and T Dwarfs. Astrophys J. 2015 Feb;799:154.
[18] Snellen IAG, Brandl BR, de Kok RJ, et al. Fast spin of the young extrasolar planet $\beta$ Pictoris b. Nature. 2014 May;509:63–65.
[19] Lagrange AM, Bonnefoy M, Chauvin G, et al. A giant planet imaged in the disk of the young star $\beta$ Pictoris. Science. 2010 Jul;329:57.

[20] Schwarz H, Ginski C, de Kok RJ, et al. The slow spin of the young sub-stellar companion GQ Lupi b and its orbital configuration. A&A. 2016;593:A74.
[21] Zhou Y, Apai D, Schneider GH, et al. Discovery of rotational modulations in the planetary-mass companion 2M1207b: intermediate rotation period and heterogeneous clouds in a low gravity atmosphere. Astrophys J. 2016 Feb;818:176.
[22] Biller BA, Vos J, Bonavita M, et al. Variability in a young, L/T transition planetary-mass object. Astrophys J Lett. 2015 Nov;813:L23.
[23] Allers KN, Gallimore JF, Liu MC, et al. The radial and rotational velocities of PSO J318.5338-22.8603, a newly confirmed planetary-mass member of the $\beta$ Pictoris moving group. Astrophys J. 2016 Mar;819:133.
[24] Marley MS, Saumon D, Goldblatt C. A patchy cloud model for the L to T dwarf transition. Astrophys J Lett. 2010 Nov;723:L117–L121.
[25] Skemer AJ, Hinz PM, Esposito S, et al. First light LBT AO images of HR 8799 bcde at 1.6 and 3.3 $\mu$m: new discrepancies between young planets and old brown dwarfs. Astrophys J. 2012 Jul;753:14.
[26] Skemer AJ, Marley MS, Hinz PM, et al. Directly imaged L-T transition exoplanets in the mid-infrared. Astrophys J. 2014 Sep;792:17.
[27] Robinson TD, Marley MS. Temperature fluctuations as a source of brown dwarf variability. Astrophys J. 2014 Apr;785:158.
[28] Tremblin P, Amundsen DS, Mourier P, et al. Fingering convection and cloudless models for cool brown dwarf atmospheres. Astrophys J Lett. 2015 May;804:L17.
[29] Tremblin P, Amundsen DS, Chabrier G, et al. Cloudless atmospheres for L/T dwarfs and extrasolar giant planets. Astrophys J Lett. 2016 Feb;817:L19.
[30] Hallinan G, Littlefair SP, Cotter G, et al. Magnetospherically driven optical and radio aurorae at the end of the stellar main sequence. Nature. 2015 Jul;523:568–571.
[31] Zapatero Osorio MR, Caballero JA, Béjar VJS, et al. Photometric variability of a young, low-mass brown dwarf. Astron Astrophys. 2003 Sep;408:663–673.
[32] Joergens V, Fernández M, Carpenter JM, et al. Rotational periods of very young brown dwarfs and very low mass stars in Chamaeleon I. Astrophys J. 2003 Sep;594:971–981.
[33] Scholz A, Eislöffel J. Rotation and accretion of very low mass objects in the $\sigma$ Ori cluster. Astron Astrophys. 2004 May;419:249–267.
[34] Caballero JA, Béjar VJS, Rebolo R, et al. Photometric variability of young brown dwarfs in the $\sigma$ Orionis open cluster. Astron Astrophys. 2004 Sep;424:857–872.
[35] Gelino CR, Marley MS, Holtzman JA, et al. L dwarf variability: I-band observations. Astrophys J. 2002 Sep;577:433–446.
[36] Dupuy TJ, Liu MC. The Hawaii infrared parallax program. I. Ultracool binaries and the L/T transition. Astrophys J Suppl. 2012 Aug;201:19.
[37] Dupuy TJ, Kraus AL. Distances, luminosities, and temperatures of the coldest known substellar objects. Science. 2013 Sep;341:1492–1495.
[38] Liu MC, Dupuy TJ, Allers KN. The Hawaii infrared parallax program. II. Young ultracool field dwarfs. Astrophys J. 2016 Dec;833:96.
[39] Kuzuhara M, Tamura M, Kudo T, et al. Direct imaging of a cold jovian exoplanet in orbit around the sun-like star GJ 504. Astrophys J. 2013 Sep;774:11.
[40] Clarke FJ, Tinney CG, Hodgkin ST. Time-resolved spectroscopy of the variable brown dwarf Kelu-1*. Mon Not R Astron Soc. 2003 May;341:239–246.
[41] Enoch ML, Brown ME, Burgasser AJ. Photometric variability at the L/T dwarf boundary. Astron J. 2003 Aug;126:1006–1016.
[42] Koen C. A search for short time-scale I-band variability in ultracool dwarfs. Mon Not R Astron Soc. 2003 Dec;346:473–482.
[43] Koen C, Matsunaga N, Menzies J. A search for short time-scale JHK variability in ultracool dwarfs. Mon Not R Astron Soc. 2004 Oct;354:466–476.
[44] Koen C. $I_C$ and $R_C$ band time-series observations of some bright ultracool dwarfs. Mon Not R Astron Soc. 2005 Jul;360:1132–1142.

[45] Koen C, Tanabé T, Tamura M, et al. $JHK_S$ time-series observations of a few ultracool dwarfs. Mon Not R Astron Soc. 2005 Sep;362:727–736.
[46] Koen C. Evidence for rapid evolution of periodic variations in an ultracool dwarf. Mon Not R Astron Soc. 2006 Apr;367:1735–1738.
[47] Maiti M, Sengupta S, Parihar PS, et al. Observation of R-band variability of L dwarfs. Astrophys J Lett. 2005 Feb;619:L183–L186.
[48] Goldman B. Ultra-cool dwarf variability. Astron Nachr. 2005 Dec;326:1059–1064.
[49] Littlefair SP, Dhillon VS, Marsh TR, et al. Observations of ultracool dwarfs with ULTRACAM on the VLT: a search for weather. Mon Not R Astron Soc. 2006 Aug;370:1208–1212.
[50] Morales-Calderón M, Stauffer JR, Kirkpatrick JD, et al. A sensitive search for variability in late L dwarfs: the quest for weather. Astrophys J. 2006 Dec;653:1454–1463.
[51] Maiti M. Observational evidence of optical variability in L dwarfs. Astron J. 2007 Apr;133:1633–1644.
[52] Bailer-Jones CAL, Mundt R. A search for variability in brown dwarfs and L dwarfs. Astron Astrophys. 1999 Aug;348:800–804.
[53] Bailer-Jones CAL, Mundt R. Variability in ultra cool dwarfs: evidence for the evolution of surface features. Astron Astrophys. 2001 Feb;367:218–235.
[54] Bailer-Jones CAL, Lamm M. Limits on the infrared photometric monitoring of brown dwarfs. Mon Not R Astron Soc. 2003 Feb;339:477–485.
[55] Bailer-Jones CAL. Spectroscopic rotation velocities of L dwarfs from VLT/UVES and their comparison with periods from photometric monitoring. Astron Astrophys. 2004 May;419:703–712.
[56] Goldman B, Cushing MC, Marley MS, et al. CLOUDS search for variability in brown dwarf atmospheres. Infrared spectroscopic time series of L/T transition brown dwarfs. Astron Astrophys. 2008 Aug;487:277–292.
[57] Artigau É, Doyon R, Lafrenière D, et al. Discovery of the brightest T Dwarf in the northern hemisphere. Astrophys J Lett. 2006 Nov;651:L57–L60.
[58] Artigau É, Bouchard S, Doyon R, et al. Photometric variability of the T2.5 brown dwarf SIMP J013656.5+093347: evidence for evolving weather patterns. Astrophys J. 2009 Aug;701:1534–1539.
[59] Radigan J, Jayawardhana R, Lafrenière D, et al. Large-amplitude variations of an L/T transition brown dwarf: multi-wavelength observations of patchy, high-contrast cloud features. Astrophys J. 2012 May;750:105.
[60] Luhman KL. Discovery of a binary brown dwarf at 2 pc from the sun. Astrophys J Lett. 2013 Apr;767:L1.
[61] Burgasser AJ, Sheppard SS, Luhman KL. Resolved near-infrared spectroscopy of WISE J104915.57-531906.1AB: a flux-reversal binary at the L dwarf/T dwarf transition. Astrophys J. 2013 Aug;772:129.
[62] Gillon M, Triaud AHMJ, Jehin E, et al. Fast-evolving weather for the coolest of our two new substellar neighbours. Astron Astrophys. 2013 Jul;555:L5.
[63] Biller BA, Crossfield IJM, Mancini L, et al. Weather on the nearest brown dwarfs: resolved simultaneous multi-wavelength variability monitoring of WISE J104915.57-531906.1AB. Astrophys J Lett. 2013 Nov;778:L10.
[64] Buenzli E, Marley MS, Apai D, et al. Cloud structure of the nearest brown dwarfs. II. High-amplitude variability for Luhman 16 A and B in and out of the 0.99 μm FeH feature. Astrophys J. 2015 Oct;812:163.
[65] Street RA, Fulton BJ, Scholz A, et al. Extended baseline photometry of rapidly changing weather patterns on the brown dwarf binary Luhman-16. Astrophys J. 2015 Oct;812:161.
[66] Mancini L, Giacobbe P, Littlefair SP, et al. Rotation periods and astrometric motions of the Luhman 16AB brown dwarfs by high-resolution lucky-imaging monitoring. Astron Astrophys. 2015 Dec;584:A104.
[67] Radigan J, Lafrenière D, Jayawardhana R, et al. Strong brightness variations signal cloudy-to-clear transition of brown dwarfs. Astrophys J. 2014 Oct;793:75.

[68] Wilson PA, Rajan A, Patience J. The brown dwarf atmosphere monitoring (BAM) project. I. The largest near-IR monitoring survey of L and T dwarfs. Astron Astrophys. 2014 Jun;566:A111.
[69] Khandrika H, Burgasser AJ, Melis C, et al. A search for photometric variability in L- and T-type brown dwarf atmospheres. Astron J. 2013 Mar;145:71.
[70] Girardin F, Artigau É, Doyon R. In search of dust clouds: photometric monitoring of a sample of late L and T dwarfs. Astrophys J. 2013 Apr;767:61.
[71] Radigan J. An independent analysis of the brown dwarf atmosphere monitoring (BAM) data: large-amplitude variability is rare outside the L/T transition. Astrophys J. 2014 Dec;797:120.
[72] Heinze AN, Metchev S, Kellogg K. Weather on other worlds. III. A survey for T dwarfs with high-amplitude optical variability. Astrophys J. 2015 Mar;801:104.
[73] Buenzli E, Apai D, Radigan J, et al. Brown dwarf photospheres are patchy: a hubble space telescope near-infrared spectroscopic survey finds frequent low-level variability. Astrophys J. 2014 Feb;782:77.
[74] Gizis JE, Burgasser AJ, Berger E, et al. Kepler monitoring of an L dwarf I. The Photometric Period and White Light Flares. Astrophys J. 2013 Dec;779:172.
[75] Gizis JE, Dettman KG, Burgasser AJ, et al. Kepler monitoring of an L dwarf. II. Clouds with multi-year lifetimes. Astrophys J. 2015 Nov;813:104.
[76] Rajan A, Patience J, Wilson PA, et al. The brown dwarf atmosphere monitoring (BAM) project – II. Multi-epoch monitoring of extremely cool brown dwarfs. Mon Not R Astron Soc. 2015 Apr;448:3775–3783.
[77] Cushing MC, Hardegree-Ullman KK, Trucks JL, et al. The first detection of photometric variability in a Y dwarf: WISE J140518.39+553421.3. Astrophys J. 2016 Jun;823:152.
[78] Leggett SK, Cushing MC, Hardegree-Ullman KK, et al. Observed variability at 1um and 4um in the Y0 brown dwarf WISEP J173835.52+273258.978. ArXiv e-prints. 2016 Jul.
[79] Esplin T, Luhman K, Cushing M, et al. Photometric monitoring of the coldest known brown dwarf with the spitzer space telescope. ArXiv e-prints. 2016 Sep;329:57.
[80] Luhman KL. Discovery of a ~250 K brown dwarf at 2 pc from the sun. Astrophys J Lett. 2014 May;786:L18.
[81] Apai D, Radigan J, Buenzli E, et al. HST spectral mapping of L/T transition brown dwarfs reveals cloud thickness variations. Astrophys J. 2013 May;768:121.
[82] Buenzli E, Apai D, Morley CV, et al. Vertical atmospheric structure in a variable brown dwarf: pressure-dependent phase shifts in simultaneous hubble space telescope-spitzer light curves. Astrophys J Lett. 2012 Dec;760:L31.
[83] Yang H, Apai D, Marley MS, et al. Extrasolar storms: pressure-dependent changes in light-curve phase in brown dwarfs from simultaneous hst and spitzer observations. Astrophys J. 2016 Jul;826:8.
[84] Morley CV, Marley MS, Fortney JJ, et al. Spectral variability from the patchy atmospheres of T and Y Dwarfs. Astrophys J Lett. 2014 Jul;789:L14.
[85] Buenzli E, Saumon D, Marley MS, et al. Cloud structure of the nearest brown dwarfs: spectroscopic variability of Luhman 16AB from the hubble space telescope. Astrophys J. 2015 Jan;798:127.
[86] Yang H, Apai D, Marley MS, et al. HST rotational spectral mapping of two L-type brown dwarfs: variability in and out of water bands indicates high-altitude haze layers. Astrophys J Lett. 2015 Jan;798:L13.
[87] Burgasser AJ, Marley MS, Ackerman AS, et al. Evidence of cloud disruption in the L/T dwarf transition. Astrophys J Lett. 2002 Jun;571:L151–L154.
[88] Cushing MC, Marley MS, Saumon D, et al. Atmospheric parameters of field L and T dwarfs. Astrophys J. 2008 May;678:1372–1395.
[89] Baraffe I, Chabrier G, Barman TS, et al. Evolutionary models for cool brown dwarfs and extrasolar giant planets. The case of HD 209458. Astron Astrophys. 2003 May;402:701–712.
[90] Morley CV, Marley MS, Fortney JJ, et al. Water clouds in Y dwarfs and exoplanets. Astrophys J. 2014 May;787:78.
[91] Kostov V, Apai D. Mapping Directly Imaged Giant Exoplanets. Astrophys J. 2013 Jan;762:47.

[92] Karalidi T, Apai D, Schneider G, et al. Aeolus: a markov chain monte carlo code for mapping ultracool atmospheres. an application on jupiter and brown dwarf HST light curves. Astrophys J. 2015 Nov;814:65.
[93] Karalidi T, Apai D, Marley MS, et al. Maps of evolving cloud structures in Luhman 16AB from HST time-resolved spectroscopy. Astrophys J. 2016 Jul;825:90.
[94] Crossfield IJM, Biller B, Schlieder JE, et al. A global cloud map of the nearest known brown dwarf. Nature. 2014 Jan;505:654–656.
[95] Vogt SS, Penrod GD, Hatzes AP. Doppler images of rotating stars using maximum entropy image reconstruction. Astrophys J. 1987 Oct;321:496–515.
[96] Rice JB, Wehlau WH, Khokhlova VL. Mapping stellar surfaces by Doppler imaging – technique and application. Astron Astrophys. 1989 Jan;208:179–188.
[97] Unruh YC. Collier Cameron A. The sensitivity of Doppler imaging to line profile models. Mon Not R Astron Soc. 1995 Mar;273:1–16.
[98] Crossfield IJM. Doppler imaging of exoplanets and brown dwarfs. Astron Astrophys. 2014 Jun;566:A130.
[99] Liu MC, Magnier EA, Deacon NR, et al. The extremely red, young L dwarf PSO J318.5338-22.8603: a free-floating planetary-mass analog to directly imaged young gas-giant planets. Astrophys J Lett. 2013 Nov;777:L20.
[100] Gizis JE, Faherty JK, Liu MC, et al. Discovery of an unusually red L-type brown dwarf. Astron J. 2012 Oct;144:94.
[101] Chauvin G, Lagrange AM, Dumas C, et al. A giant planet candidate near a young brown dwarf. Direct VLT/NACO observations using IR wavefront sensing. Astron Astrophys. 2004 Oct;425:L29–L32.
[102] Chauvin G, Lagrange AM, Dumas C, et al. Giant planet companion to 2MASSW J1207334–393254. Astron Astrophys. 2005 Aug;438:L25–L28.
[103] Lew BWP, Apai D, Zhou Y, et al. Cloud atlas: discovery of patchy clouds and high-amplitude rotational modulations in a young, extremely red L-type Brown Dwarf. Astrophys J Lett. 2016 Oct;829:L32.
[104] Macintosh B, Graham JR, Ingraham P, et al. First light of the Gemini Planet Imager. Proc Nat Acad Sci. 2014 Sep;111:12661–12666.
[105] Beuzit JL, Feldt M, Dohlen K, et al. SPHERE: a 'planet finder' instrument for the VLT. In: Ground-based and airborne instrumentation for astronomy II (Proc. SPIE; Vol. 7014, p. 18). 2008 Jun 22–28; Marseille, France. p. 701418
[106] Gagné J, Lafrenière D, Doyon R, et al. BANYAN. II. Very low mass and substellar candidate members to nearby, young kinematic groups with previously known signs of youth. Astrophys J. 2014 Mar;783:121.
[107] Gagné J, Lafrenière D, Doyon R, et al. BANYAN. V. A systematic all-sky survey for new very late-type low-mass stars and brown dwarfs in nearby young moving groups. Astrophys J. 2015 Jan;798:73.
[108] Gagné J, Faherty JK, Cruz KL, et al. BANYAN. VII. A new population of young substellar candidate members of nearby moving groups from the BASS survey. Astrophys J Suppl. 2015 Aug;219:33.
[109] Faherty JK, Riedel AR, Cruz KL, et al. Population properties of brown dwarf analogs to exoplanets. Astrophys J Suppl. 2016 Jul;225:10.
[110] Apai D, Kasper M, Skemer A, et al. High-cadence, high-contrast imaging for exoplanet mapping: observations of the HR 8799 planets with VLT/SPHERE satellite-spot-corrected relative photometry. Astrophys J. 2016 Mar;820:40.
[111] Boccaletti A, Lagage PO, Baudoz P, et al. The mid-infrared instrument for the James webb space telescope telescope, V: predicted performance of the MIRI coronagraphs. PSAP. 2015 Jul;127:633B.
[112] Line MR, Fortney JJ, Marley MS, et al. A data-driven approach for retrieving temperatures and abundances in brown dwarf atmospheres. Astrophys J. 2014 Sep;793:33.
[113] Line MR, Teske J, Burningham B, et al. Uniform atmospheric retrieval analysis of ultracool dwarfs. I. Characterizing benchmarks, Gl 570D and HD 3651B. Astrophys J. 2015 Jul;807:183.

[114] Burningham B, Marley MS, Line MR, et al. Retrieval of atmospheric properties of cloudy L dwarfs. ArXiv e-prints. 2017 Jan.
[115] Kreidberg L, Bean JL, Désert JM, et al. A precise water abundance measurement for the hot jupiter WASP-43b. Astrophys J Lett. 2014 Oct;793:L27.
[116] Benneke B. Strict upper limits on the carbon-to-oxygen ratios of eight hot jupiters from self-consistent atmospheric retrieval. ArXiv e-prints. 2015 Apr.
[117] Simon AA, Rowe JF, Gaulme P, et al. Neptune's dynamic atmosphere from Kepler K2 observations: implications for brown dwarf light curve analyses. Astrophys J. 2016 Feb;817:162.
[118] Stauffer J, Marley MS, Gizis JE, et al. Spitzer space telescope Mid-IR light curves of neptune. Astron J. 2016 Nov;152:142.
[119] Marley MS, Robinson TD. On the cool side: modeling the atmospheres of brown dwarfs and giant planets. Ann Rev of Astron Astrophys. 2015 Aug;53:279–323.
[120] Morley CV, Fortney JJ, Marley MS, et al. Neglected clouds in T and Y dwarf atmospheres. Astrophys J. 2012 Sep;756:172.
[121] Stark CR, Helling C, Diver DA. Inhomogeneous cloud coverage through the Coulomb explosion of dust in substellar atmospheres. Astron Astrophys. 2015 Jul;579:A41.
[122] Showman AP, Kaspi Y. Atmospheric dynamics of brown dwarfs and directly imaged giant planets. Astrophys J. 2013 Oct;776:85.
[123] Zhang X, Showman AP. Atmospheric circulation of brown dwarfs: jets, vortices, and time variability. Astrophys J Lett. 2014 Jun;788:L6.
[124] Mayne NJ, Baraffe I, Acreman DM, et al. The unified model, a fully-compressible, non-hydrostatic, deep atmosphere global circulation model, applied to hot Jupiters. ENDGame for a HD 209458b test case. Astron Astrophys. 2014 Jan;561:A1.